Available online at www.sciencedirect.com

SciVerse ScienceDirect

Ceramics International 38 (2012) 6203–6214

CERAMICS INTERNATIONAL

www.elsevier.com/locate/ceramint

# Synthesis of $LaB_6$ powders from $La_2O_3$, $B_2O_3$ and Mg blends via a mechanochemical route

Duygu Ağaoğulları*, İsmail Duman, M. Lütfi Öveçoğlu

*Istanbul Technical University, Faculty of Chemical and Metallurgical Engineering, Department of Metallurgical and Materials Engineering, Particulate Materials Laboratories (PML), Maslak 34469, Istanbul, Turkey*

Received 16 April 2012; accepted 23 April 2012
Available online 4 May 2012

**Abstract**

This study reports a room temperature mechanochemical route for the synthesis of $LaB_6$ powders from $La_2O_3$–$B_2O_3$–Mg blends. The synthesis reaction was driven by high-energy ball milling and was gradually examined in terms of milling duration and process control agent. Following the mechanochemical synthesis, unwanted MgO phase and Fe contamination worn off from the milling vial/balls were removed with HCl acid leaching under the effect of ultrasonic stirring. Pure $LaB_6$ powders were obtained after repeated centrifuging, repeated washing and drying. Subsequent annealing was performed in a tube furnace at 800 °C for 5 h under Ar atmosphere in order to reveal residual elements. Phase and microstructural characterizations of the milled, leached and annealed powders were performed using X-ray diffractometry (XRD), differential scanning calorimetry (DSC), scanning electron microscopy (SEM) and transmission electron microscopy (TEM) techniques. A novel route for producing fine-grained $LaB_6$ powders was accomplished with shorter reaction times resulting in higher purity.


*Keywords:* A. Powders: solid state reaction; B. Microstructure-final; B. X-ray methods; D. Borides

## 1. Introduction

Lanthanum hexaboride ($LaB_6$) is a refractory ceramic material characterized by its high melting point, high strength, high rigidity, high chemical and thermal stability, low vapor pressure (at high temperature), low electronic work function, low sputtering yield, low resistivity, low thermal expansion coefficient (in some temperature ranges), high transmission stability, excellent mechanical stability against ion bombardment, high current and voltage capability and high neutron absorbability [1–9]. It is insoluble in water and in hydrochloric acid (HCl) [1–9]. Stoichiometric $LaB_6$ samples have colors of intense purple whereas boron-rich ones ($LaB_9$) are blue [10]. However, any significant structural difference between purple and blue borides has been determined by X-ray and neutron diffraction investigations [10]. $LaB_6$ has the cubic CsCl structure with a space group of *Pm3m* symmetry, in which lanthanum ions and boron atoms respectively occupy the Cs site and octahedral site [9–11]. It is very hard due to the strong covalent bonds of boron atoms in the structure [11,12].

All these superior properties of $LaB_6$ make it a candidate for several applications such as high-energy optical systems, sensors for high resolution detectors, electrical coatings for resistors [13]. $LaB_6$ is one of the most widely used thermionic emitter which offers better performance (higher emission current density, higher brightness, higher emission stability, lower energy spread and longer service life) than tungsten cathodes in a large variety of devices such as high-resolution electron microscopes, electron beam writing units, vacuum electron beam welding machines, electron beam surface reforming and lithography devices, microwave tubes, free electron lasers and X-ray tubes [1,5,8,12,14–16]. It has the highest electronic emissivity of any known material and its performance is unaffected by the presence of nitrogen ($N_2$)

*Corresponding author. Postal address: I.T.U, Faculty of Chemical and Metallurgical Engineering, Department of Metallurgical and Materials Engineering, Ayazağa Campus, 34469 Maslak, Istanbul, Turkey.
Tel.: +90 212 285 6893; fax: +90 212 285 3427.
*E-mail addresses:* bozkurtdu@itu.edu.tr (D. Ağaoğulları), iduman@itu.edu.tr (İ. Duman), ovecoglu@itu.edu.tr (M.L. Öveçoğlu).

0272-8842/$36.00 © 2012 Elsevier Ltd and Techna Group S.r.l. All rights reserved.
http://dx.doi.org/10.1016/j.ceramint.2012.04.073

or oxygen ($O_2$) up to 700 °C [2,12,17]. Recently, $LaB_6$ nanoparticles have been proved as effective in near-infrared absorption enabling application in reduction of solar heat gain [18]. Therefore, $LaB_6$ has attracted significant interest amongst transition metal borides and rare earth hexaborides.

$LaB_6$ has been generally produced by high-temperature reactions using several diverse processes or methods such as: (i) direct solid-phase reaction of lanthanum or its oxides with elemental boron around 1800 °C, (ii) vacuum hot-pressing of lanthanum oxide and boron carbide at 1400 °C, (iii) carbothermic reduction of lanthanum oxide and boron oxide or boron at 1500 °C, (iv) arc floating zone method of lanthanum with boron at 1700 °C, (v) RF or laser heated floating zone technique, (vi) multi-float zone passage, (vii) aluminum flux method using lanthanum trichloride/lanthanum oxide and boron/boron oxide precursors above 1000 °C, (viii) catalyst-assisted or catalyst-free chemical vapor deposition (CVD) using lanthanum oxide, lanthanum trichloride or lanthanum powders and boron trichloride, boron tribromide or decaborane gases in an atmosphere of hydrogen/nitrogen/argon at 1000–1300 °C, (ix) reaction of lanthanum acetate and sodium borohydride at 900 °C, (x) reaction of hexagonal boron nitride and lanthanum-citrate-hydrate carbonized substance at 1480–1600 °C and (xi) molten salt electrolysis from oxyfluoride bath consisting $La_2O_3$–$B_2O_3$–LiF–$Li_2O$ at 800 °C under helium or nitrogen atmosphere [1,2,6–8,11–41]. In addition, $LaB_6$ nanoparticles have been prepared in a temperature range 400–500 °C via a solid-state reaction of metallic magnesium powders with sodium borohydride or boron oxide and lanthanum trichloride heptahydrate in an autoclave [1,31]. $LaB_6$ nanocrystals have also been generated by a solid-state reaction route of lanthanum trichloride and sodium borohydride at 900–1200 °C under vacuum [18]. $LaB_6$ nanopowders have been synthesized from lanthanum oxide/boron powder blends in the presence of hydrogen and/or helium in a radiofrequency thermal plasma reactor [42]. Moreover, $LaB_6$ nanocubes have been produced by low-temperature combustion synthesis of lanthanum nitrate, carbohydrazide and boron powders at 320 °C [43]. Recently, $LaB_6$ thin films have been deposited by the pulsed laser deposition technique at 850 °C and $LaB_6$ micro/nano structures have been synthesized by picosecond neodymium-doped yttrium aluminum garnet (Nd:YAG) laser [44]. Currently, there exists a number of research investigations concerning the fabrication of $LaB_6$ containing composite powders: $LaB_6$-$ZrB_2$ have been obtained from lanthanum oxide, zirconium oxide, boron carbide and carbon powder blends by hot pressing at 1300–1800 °C under vacuum [3,45]. $La_xCe_{1-x}B_6$ whiskers have been synthesized by the carbothermic vapor–liquid–solid growth mechanism of lanthanum oxide, cerium oxide and boron oxide powder blends at 1200–1800 °C [46].

Apart from the above-mentioned production techniques, an alternative room temperature method can be utilized for the synthesis of pure fine-grained $LaB_6$ powders. This method involves solid-state reactions performed by high-energy ball milling, also named as mechanochemical synthesis. This novel route enables rapid preparation for oxide dispersion strengthened alloys, amorphous materials, solid solution alloys, non-equilibrium alloys, intermetallics, nanocomposites, ceramics and advanced materials which are hard or impossible to be obtained by conventional production techniques [47,48]. The mechanism of this process is based on repeated welding, fracturing and rewelding of the reactant powder particles which result in reduction or redox reactions. Mechanochemical synthesis has been controlled by several factors such as type of mill, milling speed, milling time, ball-to-powder weight ratio (BPR), milling container, milling atmosphere, milling environment, type, size and size distribution of milling media and process control agent [47,48].

In this study, submicron/nano-scaled $LaB_6$ powders from $La_2O_3$, $B_2O_3$ and Mg powder blends were synthesized via a mechanochemical route. Effects of milling duration and process control agent on the formation of $LaB_6$ were examined. Subsequent leaching and annealing were also carried out on the selected products. This study introduces a novel, simple and room temperature process for the production of $LaB_6$ powders and consequently contributes the first results of the mechanochemically synthesized $LaB_6$ powders to the archival literature.

## 2. Experimental procedure

### 2.1. Raw materials

Raw materials used in this study were $La_2O_3$ (ABCR™, 99.99% purity), $B_2O_3$ (ETI Mine, 98% purity) and Mg (MME, 99.7% purity) powders. Magnesium was used as a strong metallic reducing agent. The crystalline phases of the raw materials were identified using a Bruker™ D8 Advanced Series X-ray diffractometer (XRD) with CuKα (1.54060 Å) radiation in the $2\theta$ range of 10–80° with 0.02° steps at a rate of 2°/min. International Center for Diffraction Data® (ICDD) powder diffraction files were utilized for the identification of crystalline phases. The XRD patterns of $La_2O_3$, $B_2O_3$ and Mg powders are respectively illustrated in Fig. 1(a)–(c) and each figure presents diffraction peaks belonging only to the pure material with no trace of impurities. Particle size measurements of the raw materials were conducted in a Malvern™ Mastersizer 2000 particle analyzer using distilled water as the aqueous media. Fig. 2(a)–(c) represent the respective particle size distributions of $La_2O_3$ [d(0.1)=7.5 μm, d(0.5)=28.8 μm, d(0.9)=67.9 μm], $B_2O_3$ [d(0.1)=268.5 μm, d(0.5)=438.8 μm, d(0.9)=708.2 μm] and Mg [d(0.1)=49.6 μm, d(0.5)=111.8 μm, d(0.9)=261.1 μm] powders. As seen in Fig. 2(a)–(c), the average particle sizes of the $La_2O_3$, $B_2O_3$ and Mg starting powders were measured as 33.6 μm, 466.9 μm and 142.7 μm, respectively. Powder blends containing stoichiometric amounts of reactants were prepared according to the overall reaction given below in Eq. (1).

$$La_2O_3 + 6B_2O_3 + 21Mg \rightarrow 2LaB_6 + 21MgO \quad (1)$$

For each run, powder batches of 6 g (1.56 g $La_2O_3$; 2.0 g $B_2O_3$; 2.44 g Mg) were weighed in a Precisa™ XB320M

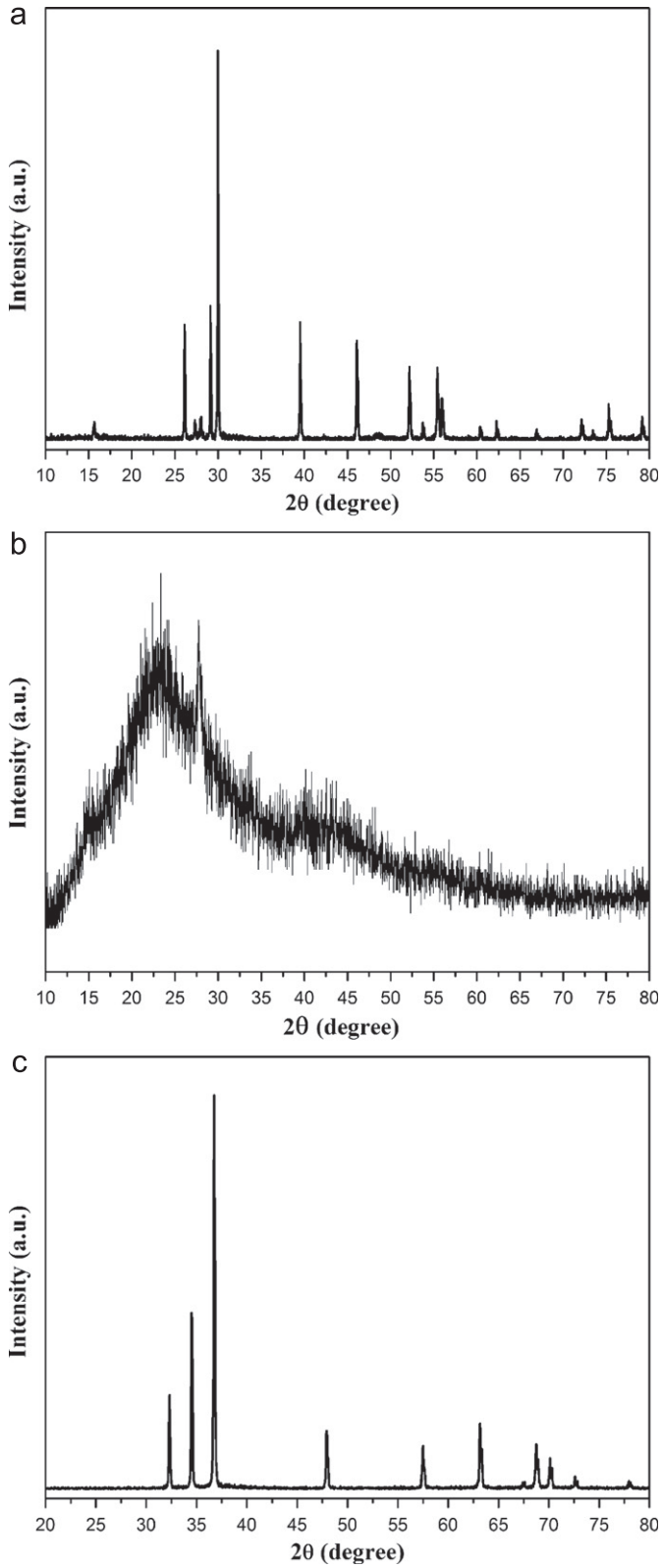


Fig. 1. XRD patterns of raw materials: (a) $La_2O_3$, (b) $B_2O_3$ and (c) Mg.

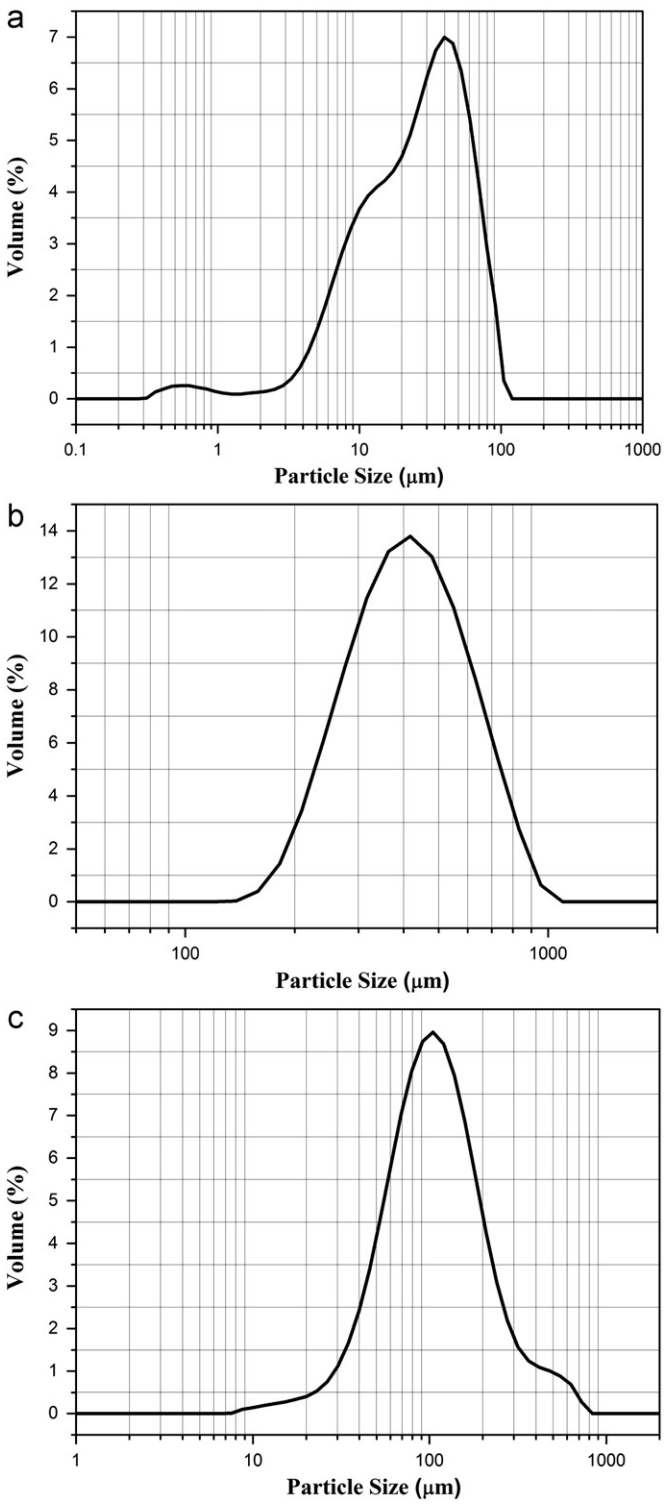


Fig. 2. Particle size distributions of raw materials: (a) $La_2O_3$, (b) $B_2O_3$ and (c) Mg.

sensitive balance (precision: 0.001 g). To investigate the effect of process control agent (PCA) on the formation mechanism of $LaB_6$, 0.5 wt% stearic acid ($C_{18}H_{36}O_2$, ZAG, 99.5% purity) was added to the powder blends in some experiments.

### 2.2. Mechanochemical synthesis

Mechanochemical synthesis experiments were carried out in a multi-axial and vibratory high-energy ball mill (Spex$^{TM}$ 8000 D Mixer/Mill) with a rotation speed of 1200 rpm. Ball-to-powder weight ratio (BPR) was chosen as 10:1 since the

required time for the complete reaction decreased with an increase in the BPR. So, it seems obvious to employ larger BPRs to prevail the effect of mechanochemical synthesis at shorter times. However, our previous studies in the synthesis of $TiB_2$ powders revealed that at higher BPRs such as 18/1, owing to high ductility of magnesium, the repeated welding, fracturing and rewelding mechanisms were disrupted [49]. Taking this into consideration, the BPR was fixed at a constant value of 10:1 for all milling runs. The milling container was a hardened steel vial with a capacity of 50 ml and the milling media was hardened steel balls with a diameter of 6 mm. The milling vial was evacuated to about $10^{-2}$ Pa and back filled with Ar gas (Linde™ 99.999% purity) in a Plaslabs™ glove box to prevent surface oxidation and contamination of powder particles. After sealing the vials, milling was continually conducted at different durations up to 25 h. The milled powders were unloaded again under Ar atmosphere in the glove-box. At least 5.4 g of powders was extracted from each vial for subsequent treatments and characterization. Additionally, as-blended (ab) powders (non-milled) were mixed and homogenized in a WAB™ T2C Turbula blender for 2 h.

### 2.3. Selective acid leaching

After sufficient milling duration, $LaB_6$ and MgO powder blends were obtained as intermediate products. Selective HCl (Merck™ 37%) leaching was applied on these products under the effect of ultrasonic stirring (Bandelin™ Sonorex). Leaching enabled the removal of the unwanted oxide phase (MgO) and the impurities (Fe, Cr, Ni) which were worn off from the milling vial and milling balls. After a series of pre-experiments, leaching parameters such as HCl concentration, solid/leachant ratio and duration were chosen respectively as 3.6 M, 1 g/10 $cm^3$ and 10 min. Pure fine-grained $LaB_6$ powders (0.223 g) were achieved from 1 g of intermediate product (milled for 5 h) after repeated centrifuging (TD3 Centrifuge, at 3500 rpm for 30 min), repeated decanting, repeated washing (in distilled water for three times) and drying (FN 500, at 120 °C for 24 h). After decantation, pH measurements (pH = 2) were made on the supernatant liquid with an universal indicator paper (Merck™ pH 0–14).

### 2.4. Annealing

High temperature annealing experiments were conducted to reveal any residual elements which could not be detected by X-ray diffraction techniques. 5 h milled and leached powders (0.1 g) were placed in a quartz boat which was inserted in a Thermoscientific™ F21130 tube furnace and annealed at 800 °C for 5 h with a heating and cooling rate of 10 °C/min under Ar gas flowing at a rate of 500 ml/min.

### 2.5. Characterization

The Gibbs free energy change and enthalpy change versus temperature curves were interpreted by HSC Chemistry™ Ver. 4.1 program. XRD investigations of the as-blended, milled, leached and annealed powders were performed in a Bruker™ D8 Advanced Series powder diffractometer using the same conditions for the raw materials. Average crystallite sizes and lattice strains of the $LaB_6$ powders were determined utilizing Bruker-AXS TOPAS V3.0 software [50]. Thermal properties of the mechanochemically synthesized powders were examined in a TA™ Instruments Q600 differential scanning calorimeter (DSC). For each run, 10 mg of powders was placed in an alumina crucible and heated up to 1100 °C at a heating rate of 10 °C/min under Ar atmosphere. Microstructural characterizations and energy dispersive spectroscopy (EDS) analyses of the milled and leached powders were carried out using a Hitachi™ TM-1000 scanning electron microscope (SEM) operated at 15 kV and a Jeol™–JEM-2000EX transmission electron microscope (TEM) operated at 160 kV. EDS results were reported as the arithmetic means of three different measurements taken from the same regions in the samples. The elements in the supernatant liquid were analyzed in a Perkin Elmer™ 1100B atomic absorption spectrometer (AAS).

## 3. Results and discussion

In order to clearly understand the formation probability of the $LaB_6$ powders, HSC Chemistry™ Ver. 4.1 program was used to calculate the reaction energetics of the ternary $La_2O_3$–$B_2O_3$–Mg system. Fig. 3 shows the Gibbs free energy change and enthalpy change versus temperature curves of the overall reaction given in Eq. (1). The reaction has a large negative free energy change indicating that it takes place spontaneously and therefore it is thermodynamically feasible at temperatures between 25 and 2000 °C. Moreover, a large negative enthalpy change of the reaction implies that a large amount of heat was released during milling due to exothermic reactions and the vial temperature increased significantly [48,52]. So, the results of the thermodynamic calculations show the possibility of a complete reaction carried out at room temperature process.

Fig. 4 illustrates the XRD patterns of the $La_2O_3$–$B_2O_3$–Mg powder blends before milling and after milling for different durations. It is evident from Fig. 4(b)–(d) that there is no reaction after milling for 1, 2 and 2.5 h since $La_2O_3$ (ICDD Card No: 071–5408, Bravais lattice: primitive hexagonal, $a=b=0.393$ nm, $c=0.614$ nm) and Mg (ICDD Card No: 035–0821, Bravais lattice: primitive hexagonal, $a=b=0.329$ nm, $c=0.521$ nm) phases are still present in the powder blend. However, the XRD patterns of the as-blended, 1 and 2 h milled powders (Fig. 4(a)–(c)) distinctly demonstrate the gradual decrease in the crystallite sizes of the $La_2O_3$ and Mg phases. No peaks belonging to the $B_2O_3$ phase can be observed in the XRD patterns of the as-blended, 1, 2 and 2.5 h milled powders (Fig. 4(a)–(d)), whose absence is attributed to its amorphous nature and further amorphization during milling. After milling for 2 h 45 min (Fig. 4(e)), the $LaB_6$ (ICDD Card No: 034–0427, Bravais lattice: primitive cubic, $a=b=c=0.416$ nm) and MgO (ICDD Card

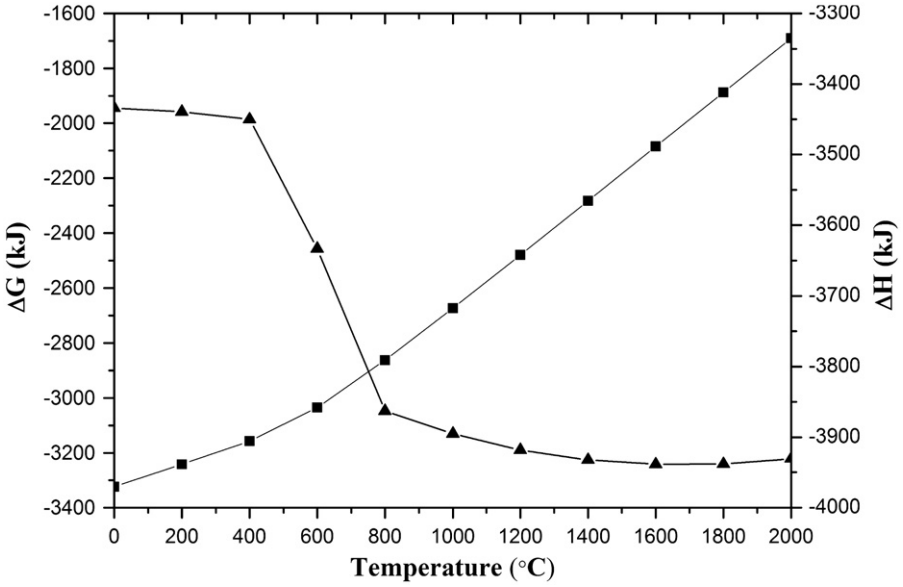


Fig. 3. Gibbs free energy change (■) and enthalpy change (▲) versus temperature curves of the overall reaction in Eq. (1).

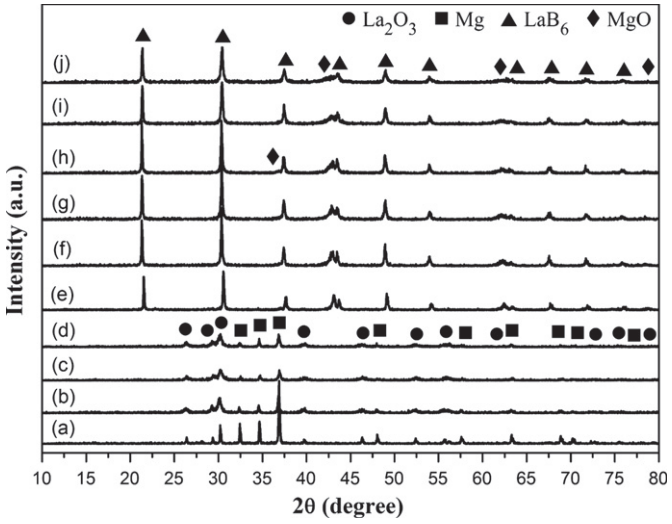


Fig. 4. XRD patterns of the $La_2O_3$–$B_2O_3$–Mg powder blends after milling for different durations: (a) 0 h, (b) 1 h, (c) 2 h, (d) 2 h 30 min, (e) 2 h 45 min, (f) 3 h, (g) 5 h, (h) 6 h, (i) 11 h and (j) 25 h.

No: 045–0946, Bravais lattice: face-centered cubic, $a=b=c=0.421$ nm) phases emerge in the microstructure as the reaction products of Eq. (1). Further milling for 15 min enables a rapid solid-state chemical reaction between the raw materials resulting in the reaction products. X-ray reflections for the $LaB_6$ phase contain ten peaks at values of 21.354°, 30.387°, 37.445°, 43.517°, 48.969°, 53.995°, 63.218°, 67.564°, 71.757°, 75.849° which are respectively indexed as (100), (110), (111), (200), (210), (211), (220), (300), (310) and (311) crystal planes (Fig. 4(e)–(j)). Additionally, the La–B binary phase diagram shows the presence of the $LaB_4$, $LaB_6$ and $LaB_9$ phases in which the $LaB_6$ is defined as the stable compound [51]. The absence of $LaB_4$ and $LaB_9$ phases in the XRD patterns and the X-ray reflections of $LaB_6$ phase have also been reported in the literature in which micro/nano structures of $LaB_6$ were synthesized by several different methods [1,2,11,18,20,31,37,42–44]. Although the $LaB_6$ formation was achieved after milling for 2 h 45 min, milling was prolonged in order to observe any probable degradation of the reaction products. Extended milling durations up to 25 h only result in the broadening of the $LaB_6$ and MgO peaks which represents decrease in their crystallite sizes (Fig. 4(e)–(j)). Therefore, the mechanochemical reaction proceeding from 2 h 45 min to 25 h is completely in agreement with the Eq. (1). There are no additional compounds between Mg–B, Mg–B–O, La–B–O, La–Mg, etc. which can be detected by the XRD analyses.

Mechanochemical synthesis is related to the repeated welding, fracturing and rewelding mechanism of the reactants and the contact points between the powder particles provide favorable conditions for the formation of the products. Two different reaction kinetics could be possible for the synthesis of the $LaB_6$ powders from the $La_2O_3$–$B_2O_3$–Mg blends. The first one may be explained by the extension of the reaction to a very small volume with each collision which results in a gradual transformation [48]. The second one could arise from the occurrence of the ignition initiated by the exothermic reactions (negative enthalpy change in Fig. 3) and attained by the critical milling duration [52]. It is considered that there is only particle refinement during milling until the ignition temperature is reached. Continuous deformation of product particles, subsequent to the mechanochemical reaction accomplished by means of ignition, again results in crystallite refinement and increase in lattice strain. Fig. 5 exhibits the average crystallite sizes and lattice strains of $LaB_6$ as a function of milling duration in the powder blends milled for 2 h 45 min, 3, 5, 6, 11 and 25 h. The average crystallite size of $LaB_6$ decreases from 82.4 nm to 42.4 nm.

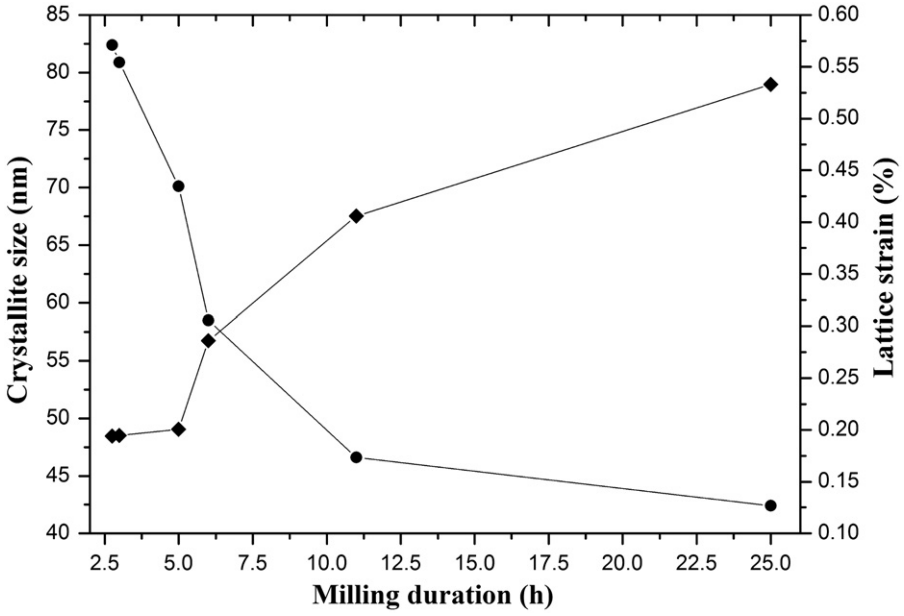


Fig. 5. Average crystallite sizes (●) and lattice strains (♦) of $LaB_6$ versus milling duration curves.

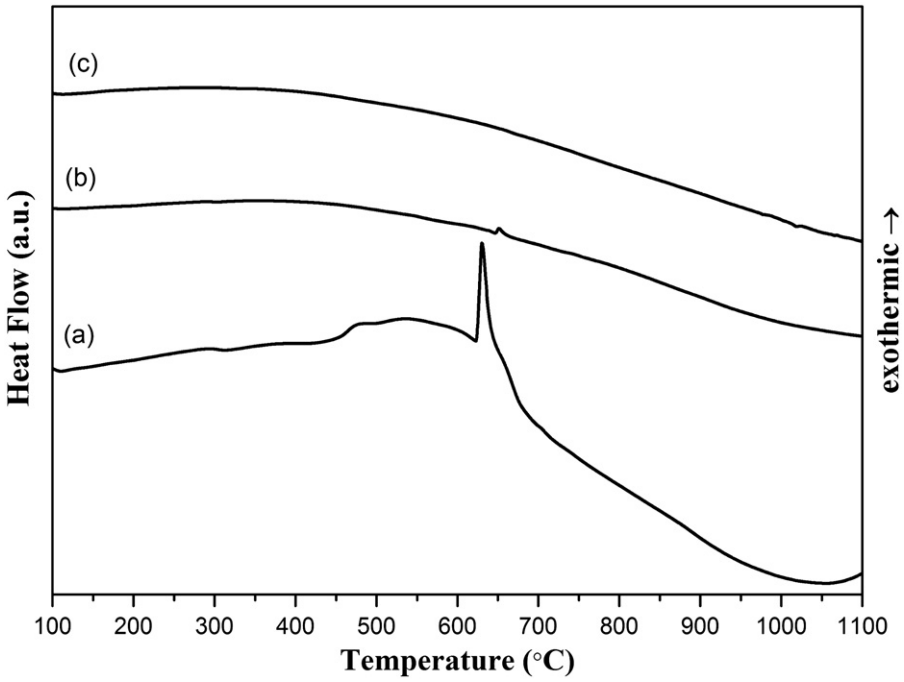


Fig. 6. DSC thermograms of the $La_2O_3$–$B_2O_3$–Mg powder blends after milling for different durations: (a) 2 h, (b) 2 h 45 min and (c) 5 h.

The decrease is sharp until 11 h of milling due to relatively effective fracturing of powder particles, however after a sufficient milling time, it slows down. In contrast to the average crystallite size, the lattice strain of $LaB_6$ increases from 0.194% to 0.533% with progressive milling. As expected, the lattice strain gives rise between 11 and 25 h milling durations. The broadening and the gradual decrease in the intensities of $LaB_6$ peaks in Fig. 4(e)–(j) correlate with pertinent average crystallite sizes and lattice strains in Fig. 5.

In order to determine the thermal behavior and the reaction completion of the $La_2O_3$–$B_2O_3$–Mg powder blends, DSC analyses were conducted on the milled (2 h, 2 h 45 min and 5 h) products (Fig. 6). The DSC curve of the 2 h milled powder given in Fig. 6(a) shows that there is only a sharp exotherm at about 630 °C with onset temperatures of 610 and 650 °C. On the basis of Fig. 4(c), 2 h milled powders contain $La_2O_3$, $B_2O_3$ and Mg phases. Although $B_2O_3$ and Mg respectively melt at 450 and 650 °C, there are any

endothermic peaks corresponding to the melting of them. Due to the identification of the exothermic peak monitored in Fig. 6(a), 2 h milled powders were heated up to 650 °C and the subsequent XRD analysis of this sample reveals $La_2O_3$, Mg and MgO phases. Thus, the sharp exothermic peak emerges in consequence of Mg oxidation. This also means that Mg was completely consumed in the dominant exothermic reaction before its melting point was reached. The DSC curve of the 2 h milled powders conforms well with ignition derived reaction kinetics since it is based on the negative enthalpy change (Fig. 3) and hence on the exothermic reactions. A study in the current literature reports the achievement of $TiO_2$, Mg and MgO main phases when $TiO_2$–$B_2O_3$–Mg powder blend (undetermined molar ratio) was treated at 630 °C [53]. As seen in Fig. 6(b), the shape and place of the main exotherm changed after 2 h 45 min milling. It became a very small and narrow exotherm between 645 and 660 °C with a maximum point of 651 °C. The temperature of the exotherm peaking point shifts about 21 °C, as a result of the comparison of Fig. 6(b) with Fig. 6(a). According to the XRD pattern in Fig. 4(e), there are $LaB_6$ and MgO phases in the 2 h 45 min milled powders. However, the exothermic peak points out the oxidation of the residual Mg in the powder blend. The contradiction between the outcomes of the XRD and DSC analyses arises from the amount of Mg which is below the XRD detection limit. Also, it can be said that mechanochemical synthesis and very small amount of remaining Mg postpone the exothermic reaction and cause the temperature shift. DSC curve of the 5 h milled powders given in Fig. 6(c) displays no exothermic peaks. This implies the completion of the reaction with no evidence of unreacted Mg, as compatible with the presence of $LaB_6$ and MgO phases in the XRD pattern in Fig. 4(g). On the basis of Figs. 4 and 6, $La_2O_3$, $B_2O_3$ and Mg powders completely reacts after 5 h milling to form $LaB_6$ and MgO.

In order to indicate the effect of milling and detect the existing phases, XRD investigations were carried out on the as-blended $La_2O_3$–$B_2O_3$–Mg powders heated to 1200 °C and rapidly cooled down to the room temperature under Ar atmosphere. Fig. 7 is a XRD pattern of the as-blended and heated powders, showing the $LaB_6$ and MgO main products with additional $LaBO_3$ (ICDD Card No: 012–0762, Bravais lattice: primitive orthorhombic, $a=0.587$ nm, $b=0.826$ nm, $c=0.511$ nm) and $Mg_3B_2O_6$ (ICDD Card No: 038–1475, Bravais lattice: primitive orthorhombic, $a=0.540$ nm, $b=0.842$ nm, $c=0.451$ nm) phases. However, as explained previously, the DSC curves of the milled powders in Fig. 6(a)–(c) do not exhibit any formation exotherms belonging to either $LaBO_3$ or $Mg_3B_2O_6$ phases. In other words, the $LaB_6$ and MgO phases which form during milling ($\geq$ 2 h 45 min) are thermally very stable and do not decompose and/or undergo phase transformation (Fig. 6(b) and (c)). It is considered that milling increases the reactivity of the components towards desired reduction reaction (Eq. (1)) since it provides particle refinement of the starting materials and thereby a more homogeneous particle size distribution throughout the powder blend can be achieved.

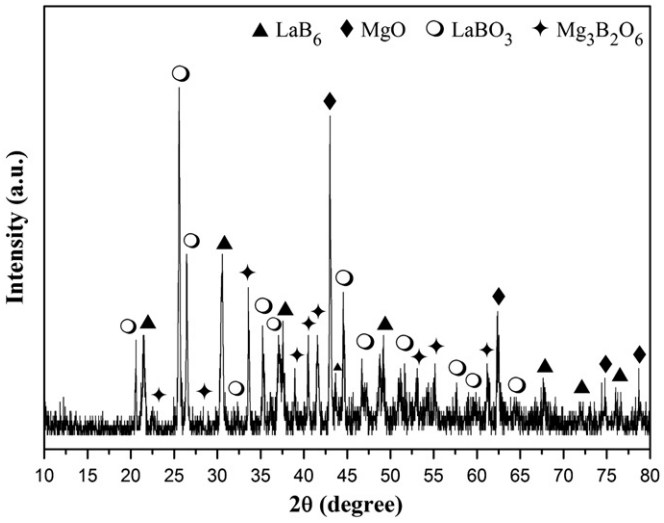


Fig. 7. XRD pattern of the as-blended $La_2O_3$–$B_2O_3$–Mg powders after heated to 1200 °C and rapidly cooled down to room temperature under Ar atmosphere.

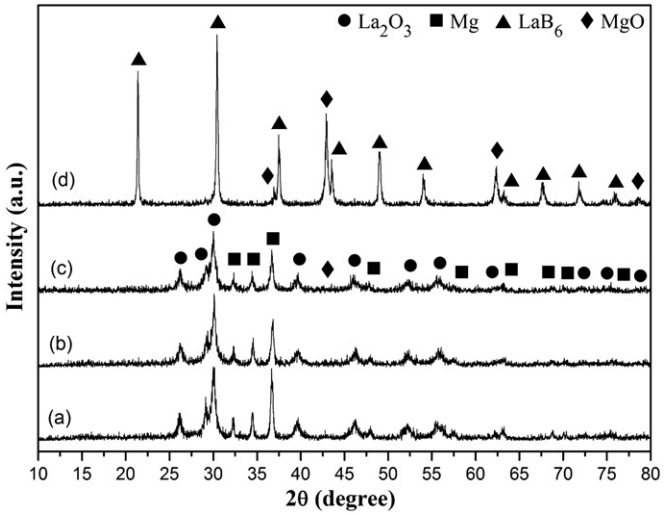


Fig. 8. XRD patterns of the PCA added $La_2O_3$–$B_2O_3$–Mg powder blends after milling for different durations: (a) 3 h, (b) 5 h, (c) 8 h and (d) 12 h.

The results indicate that if milling were not carried out on the $La_2O_3$–$B_2O_3$–Mg powder blends, the heating process had no chance of resulting complete conversion of the reactants without additional compounds. Therefore, on the basis of the XRD pattern of the as-blended and heated powders shown in Fig. 7, the significance of the mechanochemical synthesis and its effect on the reduction mechanism of $La_2O_3$ and $B_2O_3$ can be emphasized once more.

Fig. 8 shows the XRD patterns of the PCA (0.5 wt% stearic acid) added $La_2O_3$–$B_2O_3$–Mg powder blends after milling for 3, 5, 8 and 12 h. It is a known fact that process control agents act as surface-active agents and reduce the effect of cold welding by lowering the surface tension, preventing agglomeration by adsorbing on the surfaces of the powder particles and providing more homogeneous

particle size distribution [47,48,52]. As previously seen from Fig. 4(e), a milling duration of 2 h 45 min is sufficient to start the reaction for synthesizing the $LaB_6$ and MgO phases. However, no reaction takes place even after 8 h of milling (Fig. 8(a)–(c)) with the addition of 0.5 wt% stearic acid into the powder blend. There is only a very small incubation of MgO at about 42.5°. XRD patterns of the 3, 5 and 8 h milled powders in Fig. 8(a)–(c) show a gradual reduction in crystallite sizes of $La_2O_3$ and Mg. As shown in Fig. 8(d), $LaB_6$ and MgO phases emerged in the microstructure after 12 h milling in the presence of the PCA whereas the reaction was completed after 5 h milling in the absence of it (Fig. 4(g)). On the basis of this observation, it can be stated that the stearic acid slows down the reaction rate as well as decreases the particle size by inhibiting interparticle welding during collisions [48]. If only the reaction is taken as basis without considering milling duration, the effect of PCA on the crystallite size of $LaB_6$ is incontrovertible. $LaB_6$ has a crystallite size of 44.7 nm and a lattice strain of 0.332% in the PCA added powder blend milled for 12 h while the crystallite size of $LaB_6$ in the 2 h 45 min milled powders without PCA is about 82.4 nm (Fig. 5). Furthermore, the approximate value of the $LaB_6$ crystallite size in the PCA added powder blend can be reached after 11 h milling with higher lattice strain value (0.406%) in the absence of PCA. Although PCA partially eradicates the agglomeration and also adhesion problems because of its waxy structure, it prevents ignition and postpones the complete reaction. Therefore, the use of PCA cannot be considered as an economical way to synthesize $LaB_6$ powders but it nevertheless provides smaller crystallite sizes which are impossible to attain without it. On the other hand, the amount of stearic acid may be reduced to less than 0.5 wt% or the type of PCA may be changed to shorten the reaction times. Moreover, carbon, hydrogen and oxygen containing stearic acid are likely to contaminate the powder blend by introducing carbides and/or oxides into the powder particles. The probable contamination is under the detection limit of XRD since the added stearic acid is about 0.03 g for each run. Consequently, the nature and amount of the PCA and the type of the milled powder may determine the reaction time, final size, final shape and the purity of the powder particles.

According to the characterization investigations in Figs. 4, 6 and 8, 5 h was chosen as the optimum milling duration for the mechanochemical synthesis of $LaB_6$ powders and hence following processes such as leaching and annealing were conducted on the 5 h milled powder blend. Fig. 9(a)–(c) display the XRD patterns of the $La_2O_3$–$B_2O_3$–Mg powder blends after milling for 5 h (Fig. 9(a)) and those after subsequent leaching (Fig. 9(b)) and annealing (Fig. 9(c)). 1 g of 5 h milled powder blend was selectively leached with HCl under the effect of ultrasonic stirring which accelerates the interaction of powder particles in the leach solution. HCl acid was very vigorous initially for few seconds with gas evolution. After stated treatments, intense purple $LaB_6$ powders were obtained as the final product. Fig. 9(a) and

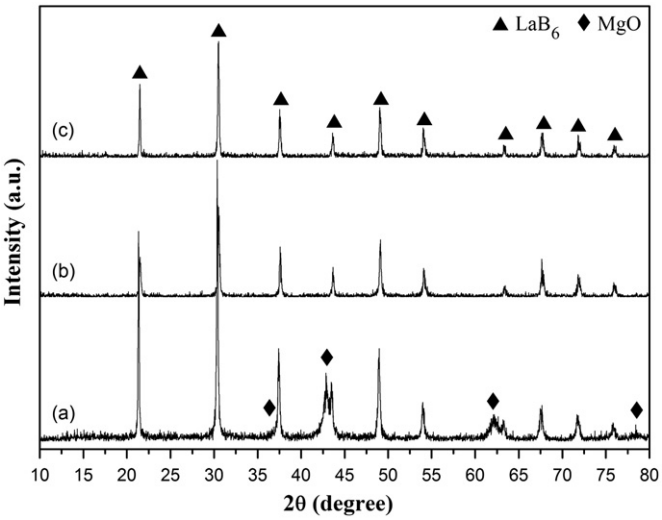


Fig. 9. XRD patterns of the $La_2O_3$–$B_2O_3$–Mg powder blends after (a) milling for 5 h, (b) milling for 5 h and leaching and (c) milling for 5 h, leaching and annealing.

(b) reveal that the unwanted by-product MgO was completely removed from the powder blend. Thus, pure $LaB_6$ powders were successfully synthesized after 5 h milling and subsequent leaching. In the XRD pattern of the 5 h milled and leached powders shown in Fig. 9(b), there is no residual magnesium chloride ($MgCl_2$) or its hydrates ($MgCl_2.xH_2O$) and magnesium hydroxychloride (MgOHCl), proving the effectiveness of the leaching parameters. Moreover, the intensities of the $LaB_6$ peaks are lower than those in the XRD pattern of the 5 h milled powder blend. This can be explained by slight dissolution of $LaB_6$ in HCl because 0.223 g residual solid was obtained instead of 0.325 g which is the theoretically calculated amount of $LaB_6$ from Eq. (1). Although the XRD patterns of the milled powders do not comprise any peaks belonging to impurities (Fe, Ni, Cr) contaminated by the milling vial and milling balls due to their very small contents, they can be removed by HCl leaching as well as MgO. It was proved by the AAS analysis of the supernatant liquid that it consists of 11.05 ppm Fe, 0.198 ppm Ni and 1.123 ppm Cr. The XRD pattern of the annealed powders in Fig. 9(c) demonstrates that final $LaB_6$ powders are sufficiently pure since it does not contain any residual elements remnant of the HCl leaching. As given in Fig. 5, the crystallite size and lattice strain of $LaB_6$ in the 5 h milled powder blend are respectively 70.1 nm and 0.201%. After leaching, the crystallite size and lattice strain reduces to 53.3 nm and to 0.029% which means that larger MgO particles and nearly the whole effect of milling on the lattice were removed. Furthermore, the crystallite size and lattice strain of $LaB_6$ increases to 139 nm and 0.052% after annealing, which is also pointed out with the higher intensities of $LaB_6$ peaks in Fig. 9(c). The lattice strain is expected to be reduced or removed by annealing. However it could be result from the appreciable increase in the crystallite size and thereby it can be considered as tolerable.

Fig. 10(a)–(c) are the respective back-scattered SEM images of the $La_2O_3$–$B_2O_3$–Mg powder blends after milling for 0, 5 and 25 h. As seen in Fig. 10(a), as-blended powders have white irregular agglomerates and dark gray leaf-like particles. EDS measurements revealed that white irregular agglomerates contain about $25.50 \pm 1.60$ wt% Mg, $23.40 \pm 3.20$ wt% B and $50.87 \pm 2.45$ O (mixture of $B_2O_3$ and Mg) and dark gray leaf-like particles involve about $84.77 \pm 2.63$ wt% La and $13.93 \pm 1.42$ wt% O, explaining respectively the mixture of $B_2O_3$ and Mg phases and the composition of $La_2O_3$ phase. According to the SEM image of the 5 h milled powder blend in Fig. 10(b), there are white rounded-shaped particles embedded in the dark gray irregular agglomerates, with sizes not larger than 800 nm. Although observable particle size is generally around 350 nm, agglomeration of the powder particles prevents the observation of smaller ones. On the basis of several EDS measurements, white particles have the composition of $65.27 \pm 2.58$ wt% La and $30.38 \pm 1.90$ wt% B and dark gray irregular agglomerates include $58.30 \pm 3.25$ wt% Mg and $37.55 \pm 3.15$ wt% O. EDS results are compatible with the calculated weight percentages of the elements in the $LaB_6$ and MgO phases. With the extension of the milling duration to 25 h, dark gray MgO agglomerates in Fig. 10(b) disappeared and replaced with the particles ranging in size between 100 and 500 nm, as obviously seen in Fig. 10(c). Besides, white $LaB_6$ particles with a maximum size of 250 nm achieve a more homogeneous distribution throughout the surface as milling duration increases. SEM images in Fig. 10(a)–(c) and their EDS measurements are in good agreement with the XRD patterns shown in Fig. 4(a), (g) and (j) and the calculated crystallite sizes shown in Fig. 5.

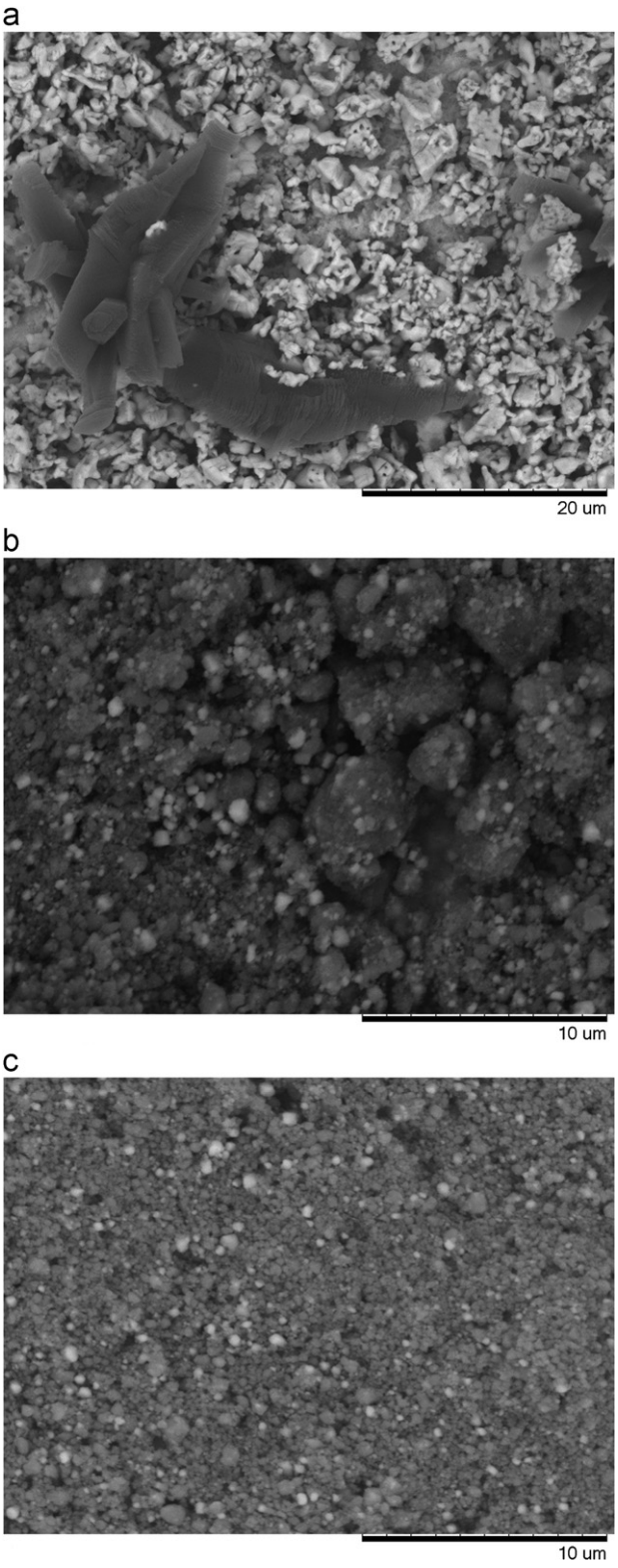


Fig. 10. Back-scattered SEM images of the $La_2O_3$–$B_2O_3$–Mg powder blends after milling for different durations: (a) 0 h, (b) 5 h and (c) 25 h.

Fig. 11(a) is a back-scattered SEM image of the $La_2O_3$–$B_2O_3$–Mg powder blend after milling for 5 h and leaching. According to this figure, the 5 h milled and leached powders have a homogeneous particle size distribution and consist of equiaxed particles smaller than 500 nm. Distinct particle size reduction of the leached powders can be obviously seen by comparing them with Fig. 10(b). The general EDS analysis of this sample indicates that the synthesized powders do not involve any residual element or contamination since only $67.40 \pm 1.83$ wt% La and $32.90 \pm 0.80$ wt% B were present in the microstructure. Fig. 11(b)–(d) are the bright-field (BF), dark-field (DF) and selected area diffraction pattern (SADP, from the white-circled region of BF image) micrographs taken from the $La_2O_3$–$B_2O_3$–Mg powder blend after milling for 5 h and leaching. Fig. 11(b) is a BF image taken from a general region showing agglomerates comprising polygonal/spheroidal-shaped particles in sizes varying between 75 and 300 nm. Spheroidal-shaped $LaB_6$ grains ranging in size between 25 and 60 nm can be unambiguously identified from the micrographs in Fig. 11(c) and (d). These findings conform with the XRD (Fig. 9(b)) and AAS analyses and the average crystallite size reduction from 5 h milled powders to leached powders was also supported by the SEM and TEM images. Consequently, $LaB_6$ powders with fine microstructure were synthesized and can be further processed to various shapes of rods, tubes, wires, slabs, disks and special designated forms and also can be further used as precursors of composites.

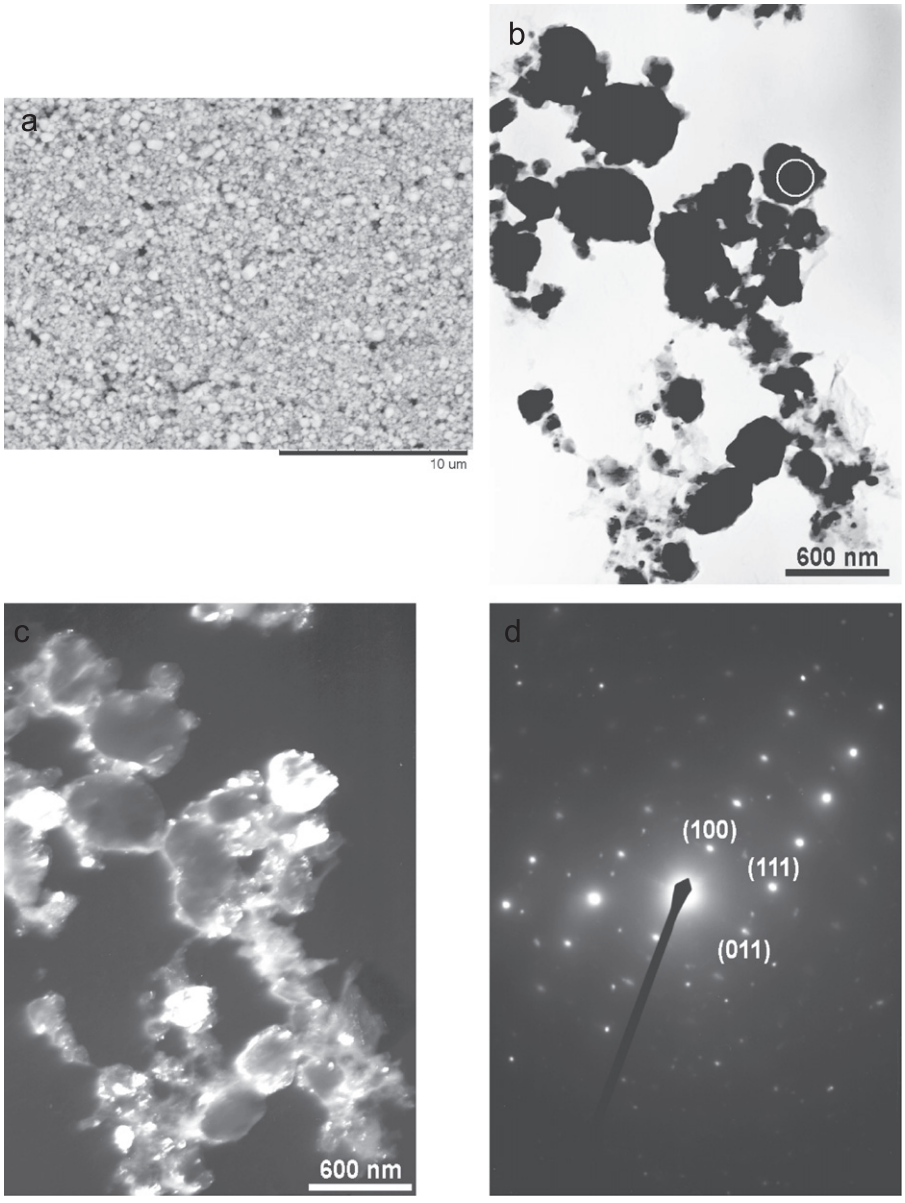


Fig. 11. Micrographs of the $La_2O_3$–$B_2O_3$–Mg powder blend after milling for 5 h and leaching: (a) Back-scattered SEM image, (b) Bright-field (BF) TEM image, (c) Dark-field (DF) TEM image and (d) Selected area diffraction pattern (SADP) revealing the presence of $LaB_6$ particles ranging in size between 75 and 300 nm. Objective aperture is on $(0\bar{1}\bar{1})$, camera length is 100 cm and zone axis is $[0\bar{1}1]$.

## 4. Conclusions

Based on the results reported in the present study, the following conclusions can be drawn:

- A novel and simple process for synthesizing $LaB_6$ powders was achieved by mechanochemical reaction of powder blends containing stoichiometric amounts of $La_2O_3$, $B_2O_3$ and Mg powders.
- The formation reaction of the $LaB_6$ and MgO phases took place after 2 h 45 min milling and completed after 5 h milling in Spex 8000 D Mixer/Mill with a 10/1 ball-to-powder weight ratio. No peaks of Mg–B, Mg–B–O, La–B–O and La–Mg or other unstable La–B can be detected in the XRD patterns of the milled products.
- The addition of stearic acid as process control agent has a negative effect on the milling duration due to the postponement of the chemical reaction. However, it has a positive effect on the average crystallite size and lattice strain of $LaB_6$ and also their agglomeration.
- Subsequent leaching which was done at 3.6 M HCl concentration with 1 g/10 $cm^3$ solid/leachant ratio during 10 min enables to obtain pure $LaB_6$ powders with a particle size between 75 and 300 nm and with a grain size between 25 and 60 nm. The purity of $LaB_6$ powders was also proved by the annealing of the 5 h milled and leached powders at 800 °C for 5 h.

## Acknowledgements

This study was supported by "The Scientific and Technological Research Council of Turkey (TÜBİTAK)" with the project title "Synthesis of Lanthanum, Cerium and Samarium Borides by Solid-State Reaction at Room Temperature" and with the project number 109M364. The authors wish to thank Aziz Genç for his help during TEM characterizations. We would also like to acknowledge the State Planning Organization (DPT) for funding the projects entitled "Advanced Technologies in Engineering" with the project number 2001K120750 and "Development of Al–Cu Based Metal Matrix Composites via Powder Metallurgy Techniques" with the project number 90189 out of which the main infrastructure of the Particulate Materials Laboratories was founded.

## References

[1] M. Zhang, L. Yuan, X. Wang, H. Fan, X. Wang, X. Wu, H. Wang, Y. Qian, A low-temperature route for the synthesis of nanocrystalline $LaB_6$, Journal of Solid State Chemistry 181 (2008) 294–297.
[2] J. Xu, Y. Zhao, C. Zou, Self-catalyst growth of $LaB_6$ nanowires and nanotubes, Chemical Physics Letters 423 (2006) 138–142.
[3] R. Gao, G. Min, H. Yu, S. Zheng, Q. Lu, J. Han, W. Wang, Fabrication and oxidation behavior of $LaB_6$-$ZrB_2$ composites, Ceramics International 31 (2005) 15–19.
[4] A.E. Baranovskiy, G.E. Grechnev, V.D. Fil, T.V. Ignatova, A.V. Logosha, A.S. Panfilov, I.V. Svechkarev, N.Y. Shitsevalova, V.B. Filippov, O. Eriksson, Electronic structure, bulk and magnetic properties of $MB_6$ and $MB_{12}$ borides, Journal of Alloys and Compounds 442 (2007) 228–230.
[5] X. Wang, Y. Jiang, Z. Lin, K. Qi, B. Wang, Field emission characteristics of single crystal $LaB_6$ field emitters fabricated by electrochemical etching method, Journal of Physics D: Applied Physics 42 (2009) 1–4.
[6] L.W. Swanson, D.R. McNeely, Work functions of the (001) face of the hexaborides of Ba, La, Ce and Sm, Surface Science 83 (1979) 11–28.
[7] P.I. Loboda, H.P. Kysla, S.M. Dub, O.P. Karasevska, Mechanical properties of the monocrystals of lanthanum hexaboride, Materials Science 45 (2009) 108–113.
[8] C.H. Chen, T. Aizawa, N. Iyi, A. Sato, S. Otani, Structural refinement and thermal expansion of hexaborides, Journal of Alloys and Compounds 366 (2004) L6–8.
[9] C.L. Perkins, M. Trenary, T. Tanaka, S. Otani, X-ray photoelectron spectroscopy investigation of the initial oxygen adsorption sites on the $LaB_6$ (100) surface, Surface Science 423 (1999) L222–228.
[10] M.J. McKelvy, L. Eyring, E.K. Storms, Analytical and structural analysis of the lanthanum-deficient lanthanum hexaboride, The Journal of Physical Chemistry 88 (1984) 1785–1790.
[11] R.K. Selvan, I. Genish, I. Perelshtein, J.M.C. Moreno, A. Gedanken, Single step, low-temperature synthesis of submicron-sized rare earth hexaborides, Journal of Physical Chemistry C 112 (6) (2008) 1795–1802.
[12] C.H. Wen, T.M. Wu, W.C. Wei, Oxidation kinetics of $LaB_6$ in oxygen rich conditions, Journal of the European Ceramic Society 24 (2004) 3235–3243.
[13] G. Balakrishnan, M.R. Lees, D.M.K. Paul, Rare earth hexaborides: large single crystals, Journal of Magnetism and Magnetic Materials 272–276 (2004) 601–602.
[14] H. Ahmed, P.L. Kanitkar, C.V. Dharmadhikari, D.S. Joag, A new method for melting and recrystallization of lanthanum hexaboride ($LaB_6$) for preparing field emitters, Journal of Physics E: Scientific Instruments 9 (1976) 4–5.
[15] H. Zhang, B. Tang, P.W. Zhu, Q. Zhang, O. Zhou, L.C. Qin, Fabrication of lanthanum hexaboride single nanowire field emitter and their field emission properties, T. Mrs. Jap. 32 (2007) 747–750.
[16] H. Zhang, J. Tang, Q. Zhang, G. Zhao, G. Yang, J. Zhang, O. Zhou, L.C. Qin, Field emission of electrons from single $LaB_6$ nanowires, Advanced Materials (Weinheim, Germany) 18 (2006) 87–91.
[17] M. Futamoto, M. Nakazawa, U. Kawabe, Thermionic emission properties of hexaborides, Surface Science 100 (1980) 470–480.
[18] Y. Yuan, L. Zhang, L. Liang, K. He, R. Liu, G. Min, A solid-state reaction route to prepare $LaB_6$ nanocrystals in vacuum, Ceramics International 37 (2011) 2891–2896.
[19] S.Q. Zheng, G.H. Min, Z.D. Zou, X.Z. Wang, J.D. Han, Synthesis of $LaB_6$ powder by reaction in $La_2O_3$-$B_4C$ system, Acta Metallurgica Sinica 37 (2001) 419–422.
[20] W. Wenyuan, X. Jingyu, P. Kewu, T. Ganfeng, High temperature chemical reaction of $La_2O_3$ in $H_3BO_3$-C system, Journal of Rare Earths 25 (2007) 282–285.
[21] B.J. Curtis, H. Graffenberger, The floating zone crystal growth of lanthanum hexaboride, Materials Research Bulletin 1 (1966) 27–31.
[22] T. Tanaka, E. Bannai, S. Kawai, T. Yamane, Growth of high purity $LaB_6$ single crystals by multi-float zone passage, Journal of Crystal Growth 30 (1975) 193–197.
[23] J.D. Verhoeven, E.D. Gibson, M.A. Noack, R.J. Conzemius, An arc floating zone technique for preparing single crystal lanthanum hexaboride, Journal of Crystal Growth 36 (1976) 115–120.
[24] K. Takagi, M. Ishii, Growth of $LaB_6$ single crystals by a laser floating zone method, Journal of Crystal Growth 40 (1977) 1–5.
[25] S. Otani, S. Honma, T. Tanaka, Y. Ishizawa, Preparation of neodymium-substituted $LaB_6$ single crystals by the floating zone method, Journal of Alloys and Compound 179 (1992) 201–205.
[26] S. Otani, S. Honma, Y. Ishizawa, Preparation of $LaB_6$ single crystals by the floating zone method, Journal of Alloys and Compound 193 (1993) 286–288.
[27] S. Otani, T. Tanaka, Y. Ishizawa, Crystal quality and high temperature hardness of $LaB_6$ crystals prepared by the floating zone method, Journal of Alloys and Compound 202 (1993) L25–28.
[28] S. Otani, S. Honma, Y. Yajima, Y. Ishizawa, Preparation of $LaB_6$ single crystals from a boron-rich molten zone by the floating zone method, Journal of Crystal Growth 126 (1993) 466–470.
[29] S. Otani, H. Nakagawa, Y. Nishi, N. Kieda, Floating zone growth and high temperature hardness of rare-earth hexaboride crystals: $LaB_6$, $CeB_6$, $PrB_6$, $NdB_6$, and $SmB_6$, Journal of Solid State Chemistry 154 (2000) 238–241.
[30] P. Peshev, A thermodynamic analysis of lanthanum hexaboride crystal preparation from aluminum flux with the use of compound precursors, Journal of Solid State Chemistry 133 (1997) 237–242.
[31] X.H. Ji, Q.Y. Zhang, J.Q. Xu, Y.M. Zhao, Rare-earth hexaborides nanostructures: recent advances in materials, characterization and investigations of physical properties, Progress in Solid State Chemistry 39 (2011) 51–69.
[32] T. Niemyski, E. Kierzek-Pecold, Crystallization of lanthanum hexaboride, Journal of Crystal Growth 3-4 (1968) 162–165.
[33] S. Motojima, Y. Takahashi, K. Sugiyama, Chemical vapor growth of $LaB_6$ whiskers and crystals having a sharp tip, Journal of Crystal Growth 44 (1978) 106–109.
[34] E.I. Givargizov, L.N. Obolenskaya, Controlled growth of $LaB_6$ whiskers by the vapor-liquid-solid mechanism, Journal of Crystal Growth 51 (1981) 190–194.
[35] E.I. Givargizov, L.N. Obolenskaya, Regular arrays of $LaB_6$ whiskers grown on single crystal substrates by the vapour-liquid-solid method, Journal of Less-Common Metals 117 (1986) 97–103.
[36] J.R. Brewer, N. Deo, Y.M. Wang, C.L. Cheung, Lanthanum hexaboride nanoobelisks, Chemistry of Materials: a Publication of the American Chemical Society 19 (2007) 6379–6381.
[37] J.Q. Xu, Y.M. Zhao, Q.Y. Zhang, Enhanced electron field emission from single-crystalline $LaB_6$ nanowires with ambient temperature, Journal of Applied Physics 104 (2008) 124306-1–124306-4.

[38] M. Shiota, M. Tsutsumi, K. Uchida, Synthesis of $LaB_6$ from BN and lanthanum-citrate-hydrate, Journal of Materials Science 15 (1980) 1987–1992.
[39] I.V. Zubeck, R.S. Feigelson, R.A. Huggins, P.A. Pettit, The growth of lanthanum hexaboride single crystals by molten salt electrolysis, Journal of Crystal Growth 34 (1976) 85–91.
[40] H. Scholz, W. Bauhofer, K. Ploog, Preparation of lanthanum hexaboride by electrolysis and measurements of the Raman-active phonons, Solid State Communications 18 (1976) 1539–1542.
[41] M. Kamaludeen, I. Selvaraj, A. Visuvasam, R. Jayavel, $LaB_6$ crystals from fused salt electrolysis, Journal of Materials Chemistry 8 (1998) 2205–2207.
[42] J. Szépvölgyi, I. Mohai, Z. Károly, L. Gál, Synthesis of nanosized ceramic powders in a radiofrequency thermal plasma reactor, Journal of the European Ceramic Society 28 (2008) 895–899.
[43] R. Kanakala, G. Rojas-George, O.A. Graeve, Unique preparation of hexaboride nanocubes: a first example of boride formation by combustion synthesis, Journal of the American Ceramic Society 93 (2010) 3136–3141.
[44] D.J. Late, V.R. Singh, S. Sinha, M.A. More, K. Dasgupta, D.S. Joag, Synthesis of $LaB_6$ micro/nano structures using picosecond (Nd: YAG) laser and its field emission investigations, Applied Physics A: Materials Science and Processing 97 (2009) 905–909.
[45] A. Spring, W. Guo, G. Zhang, P. Wang, V.D. Krstic, Fabrication and characterization of $ZrB_2$-based ceramic using synthesized $ZrB_2$-$LaB_6$ powder, Journal of the American Ceramic Society 91 (2008) 2763–2765.
[46] M. Carlsson, F.J. Garcia-Garcia, M. Johnsson, Synthesis of $La_x$-$Ce_{1-x}B_6$ whiskers, Journal of Materials Science 40 (2005) 2991–2994.
[47] M.S. El-Eskandarany, Mechanical Alloying for Fabrication of Advanced Engineering Materials, Noyes Publications, New York, 2001.
[48] C. Suryanarayana, Mechanical alloying and milling, Progress In Materials Science 46 (2001) 1–184.
[49] D. Agaogullari, F. Aynibal, O.C. Demirhan, I. Duman, Synthesis of titanium diboride by solid-state reaction between $TiO_2$, $B_2O_3$ and Mg, Seres'09: Proceedings of the 1st International Ceramic, Glass, Porcelain Enamel, Glaze and Pigment Congress, 12–14 October 2009, Eskişehir, Turkey, pp. 1161–1173.
[50] A.A. Kern, A.A. Coelho, Bruker-AXS TOPAS V.3.0. 2006, 〈www.brukeraxs.com〉.
[51] M.E. Schlesinger, P.K. Liao, K.E. Spear, The B-La (boron-lanthanum) system, Journal of Phase Equilibria 20 (1999) 73–78.
[52] B. Murty, R. Ranganathan, Novel materials synthesis by mechanical alloying/milling, International Materials Reviews 43 (1998) 101–141.
[53] W. Weimin, F. Zhengyi, W. Hao, Y. Runzhang, Chemistry reaction processes during combustion synthesis of $B_2O_3$-$TiO_2$-Mg system, Journal of Materials Processing Technology 128 (2002) 162–168.